HHS Public Access

Author manuscript

Magn Reson Med. Author manuscript; available in PMC 2014 November 08.

Published in final edited form as:

Magn Reson Med. 2014 March ; 71(3): 1158–1165. doi:10.1002/mrm.24775.

Bone marrow fat quantification in the presence of trabecular bone: initial comparison between water-fat imaging and single-voxel MRS

Dimitrios C. Karampinos[1,2], **Gerd Melkus**[1], **Thomas Baum**[2], **Jan S. Bauer**[2], **Ernst J. Rummeny**[2], and **Roland Krug**[1]

[1]Department of Radiology and Biomedical Imaging, University of California, San Francisco, San Francisco, CA, USA

[2]Department of Diagnostic and Interventional Radiology, Technische Universität München, Munich, Germany

Abstract

Purpose—The purpose of the present study was to test the relative performance of chemical shift-based water-fat imaging in measuring bone marrow fat fraction in the presence of trabecular bone, having as reference standard the single-voxel magnetic resonance spectroscopy (MRS).

Methods—Six-echo gradient echo imaging and single-voxel MRS measurements were performed on the proximal femur of seven healthy volunteers. The bone marrow fat spectrum was characterized based on the magnitude of measurable fat peaks and an a priori knowledge of the chemical structure of triglycerides, in order to accurately extract the water peak from the overlapping broad fat peaks in MRS. The imaging-based fat fraction results were then compared to the MRS-based results both without and with taking into consideration the presence of short T_2* water components in MRS.

Results—There was a significant underestimation of the fat fraction using the MRS model not accounting for short T_2* species with respect to the imaging-based water fraction. A good equivalency was observed between the fat fraction using the MRS model accounting for short T_2* species and the imaging-based fat fraction (R^2=0.87).

Conclusion—The consideration of the short T_2* water species effect on bone marrow fat quantification is essential when comparing MRS-based and imaging-based fat fraction results.

Keywords

red bone marrow; fat quantification; water-fat separation; magnetic resonance imaging (MRI); magnetic resonance spectroscopy (MRS); short T_2* species

Corresponding Author Address: Dimitrios C. Karampinos, Department of Diagnostic and Interventional Radiology, Klinikum rechts der Isar, Ismaninger Str. 22, 81675 Munich, Germany, phone: +49-89-4140-7220, dimitrios.karampinos@tum.de.

INTRODUCTION

Bone marrow fat quantification has been proposed as a useful tool in understanding the relationship between osteoporosis and bone marrow adiposity (1-3) and in characterizing cellularity for radiation dosimetry in cancer patients (4). Single-voxel MR spectroscopy has been the technique traditionally used to measure fat content in localized regions of the vertebral bodies and the proximal femur (2,3,5,6). However, the distribution of bone marrow fat content can be spatially heterogeneous and there is a growing interest in applying chemical shift-based water fat imaging techniques for measuring bone marrow fat content with high spatial resolution (4).

Quantitative water-fat imaging techniques have been emerging (7,8) and have shown excellent agreement with single-voxel MRS in measuring proton density fat fraction (PDFF) maps in different body parts (9-12), after consideration of multiple confounding factors, including main magnetic field inhomogeneity effects (13), the presence of multiple peaks in the fat spectrum (14,15), T_2* effects (14,16), T_1 effects (14,17,18), eddy current effects (19,20) and the presence of susceptibility-induced fat resonance shifts (21). However, a study of the relationship of bone marrow fat content measurements between water-fat imaging and single-voxel MRS has not been performed before. Such a study becomes particularly relevant in the presence of trabecular bone.

The presence of trabecular bone complicates fat quantification in bone marrow using both single-voxel MR spectroscopy and water-fat imaging. In single-voxel MRS, trabecular bone shortens the T_2* of water and fat components, broadening the linewidths of all the associated peaks and hindering the accurate extraction of the water peak next to the surrounding fat peaks in the MR spectrum (5,6). In water-fat imaging, trabecular bone in general shortens the T_2* of water and fat components inducing a rapid decay of the measured gradient echo signal with echo time (TE) (14,16).

Measurement of red bone marrow fat content in the presence of trabecular bone can be also affected by the presence of signal from short T_2* water components. Short T_2* water components include water molecules bound to the bone mineral matrix as well as free water molecules with short T_2* induced by different potential sources, including the presence of trabecular bone pores with different scales, the presence of macromolecules (e.g. proteins) within the hematopoietic red blood cells and the presence of paramagnetic ions (e.g. iron). Water components with short T_2* and short T_2 would have negligible contribution to the MR signal of measurements using either clinically accessible gradient echo imaging or single-voxel MRS. Water components with short T_2* (below 2 ms at 3T) and long T_2 would have small or negligible contribution to the MR signal at the TEs of clinically accessible gradient echo sequences, but would contribute to the MR spectra acquired using single-voxel MRS by inducing broad baseline peaks.

The present study aims to compare bone marrow proton density fat fraction measurements in the presence of trabecular bone using clinically accessible water-fat imaging with the fat fraction measurements from single-voxel MRS, which has been previously extensively used to measure bone marrow fat content. To overcome the difficulty of accurately extracting the

water peak from the overlapping fat peaks in MRS, the bone marrow fat MR spectrum is first characterized based on the magnitude of measurable fat peaks and an a priori knowledge of the chemical structure of triglycerides, as previously proposed in (22). To address the effect of short T_2* water components on fat quantification, the imaging-based fat fraction results are then compared to the MRS-based results both without and with taking into consideration the presence of short T_2* water components.

METHODS

MR measurements

The left proximal femur of seven young healthy volunteers (4 males and 3 females, with age=25.3±5.1 years) was scanned on a 3 T whole-body scanner (MR750, GE Healthcare, Waukesha, Wisconsin, USA) using an 8-channel cardiac coil. The study was approved by our Institutional Review Board. The MR exam consisted of a coronal 3D spoiled gradient echo (SPGR) sequence and multiple repetitions of an MRS sequence, applied in different bone marrow regions of the proximal femur.

A six-echo 3D SPGR sequence was used for chemical shift-based water-fat separation with the following imaging parameters: 2 echoes per TR and mono-polar read-out gradients (23), $TR/TE_{min}/\Delta TE$=9.8/2.1/1.0 ms, FOV=12×12 cm^2, acquisition matrix=150×150, slice thickness=2 mm, slice locations=32, receiver bandwidth=62.5 kHz, frequency direction=L/R, no phase-wrap on, N_{avg}=2. A flip angle of 2° was used to minimize T_1-bias effects.

Based on the proton density fat fraction map derived using the chemical shift-based water-fat separation, 2-5 locations (from regions in the neck, greater trochanter and head of the proximal femur) were selected per subject to perform single-voxel (12×12×12 mm^3) MRS (resulting in a total of 25 acquired locations from the 7 scanned subjects) using a STEAM sequence with parameters: TR=6 s, TE=15/20/25/30 ms (STEAM with short TEs to reduce J-coupling effects), 9 averages per TE, 4096 data points, 5 kHz acquisition bandwidth, 2.4 kHz RF pulse bandwidth, no water suppression and no regional saturation bands. Two sets of acquisitions at two different center frequencies (one set on the main fat peak and one set on the water peak) were performed to correct for chemical shift displacement effects due to the finite bandwidth of the employed RF pulses used in the MRS voxel localization.

Fat spectrum characterization

Spectra were fitted using Gaussian lineshapes and frequency-based methods based on in house-built routines written in MATLAB (Mathworks, Natick, MA). Fig. 1a shows a typical bone marrow fat spectrum with fat peaks observed at spectral locations at 0.9, 1.30, 1.59, 2.00, 2.25, 2.77, 4.2 and 5.31 ppm. The letters A, D, E and F were assigned to peaks at 0.9 ppm ($-(CH_2)_n-C\mathbf{H}_3$), 2.77 ppm ($-CH=CH-C\mathbf{H}_2-CH=CH-$), 4.2 ppm ($-C\mathbf{H}_2-O-CO-$), and 5.31 ppm ($-C\mathbf{H}=C\mathbf{H}-$) respectively. The letter B was assigned to the superposition of peaks at 1.30 ppm ($-(C\mathbf{H}_2)_n-$) and 1.59 ppm ($-CO-CH_2-C\mathbf{H}_2-$), and the letter C was assigned to the superposition of peaks at 2.00 ppm ($-C\mathbf{H}_2-CH=CH-C\mathbf{H}_2-$) and 2.25 ppm ($-CO-C\mathbf{H}_2-CH_2-$). The spectra acquired with center frequency at the main fat peak were

used to fit fat peaks A, B, C and D (Fig. 1a). A common linewidth was assumed for all peaks contributing to fat peaks A, B, C and D.

The relationship between the computed area of peak C and the computed area of peaks A+B was studied for all spectra. The relationship between the computed area of peak D and the computed area of peak C was studied for spectra with fat peak linewidth smaller than 0.4 ppm. The two derived linear regression coefficients and the model of chemical structure of the triglycerides were then used to estimate the number of double bonds (ndb) and the number of methylene-interrupted double bonds (nmidb), adopting the framework introduced by Hamilton (22). Based on the computed values for ndb and nmidb and assuming a reasonable value for the triglyceride chain length (CL), the relative areas of all fat peaks were determined. In the spectroscopy-based fat quantification, the computed relative fat peak area results were used to fit the fat peaks overlapping with the water peak, by constraining their area to the area of the main fat peak. In the imaging-based fat quantification, the computed relative fat peak area results were used to form the pre-calibrated fat spectrum employed in the signal model.

Spectroscopy-based fat quantification

Chemical shift displacement effects depend on the spectral location of the measured peak relative to the center frequency of the MRS acquisition. Chemical shift displacement effects are expected to be small for fat peaks A, B, C and D in the MRS acquisition centered on the main fat peak. Chemical shift displacement effects are expected to be small for the water peak and fat peaks E and F in the MRS acquisition centered on the water peak. Fat spectra minimally affected by chemical shift displacement effects were thus derived by combining the spectrum acquired with center frequency at the main fat peak for chemical shift values lower than 3 ppm and the spectrum acquired with center frequency at the water peak for chemical shift values higher than 3 ppm. Peak fitting was performed by constraining the area of peaks E and F at a given ratio of peak A+B, based on the triglyceride chemical structure determined in the fat spectrum characterization step (see Results section). A common linewidth was assumed for all peaks contributing to fat peaks A, B, C and D and independent linewidth values were fitted for fat peaks E and F and the water peak, resulting in a total number of four linewidths as free variables. Fat peak locations were allowed to vary by ±0.05 ppm and water peak locations were allowed to vary by ±0.25 ppm. Peak fitting was performed for the spectra at individual TEs. T_2 correction was then performed using non-linear least squares fitting, assuming the same T_2 relaxation time value for all fat peaks and a different value for the water T_2 relaxation time. The mean water and main fat peak linewidths were computed for spectra with an MRS-determined fat fraction below 85% (to assure the presence of a strong water peak). A two-sided t test at a significance level of $p=0.05$ was used to determine whether the relative difference between the linewidths of water and main fat peak was statistically different from 0.

To investigate the effect of short T_2* water species, MRS fitting was performed for the combined spectra, formed to minimize chemical shift displacement effects: (i) by considering a single water peak (method not accounting for short T_2* species) and (ii) by considering a narrow and a broad water peak (method accounting for short T_2* species). The

fat fraction using the method not accounting for short T_2* species was determined as the ratio of all the fat peaks (A, B, D, E and F) area with the sum of all the fat peaks and the single water peak area. The fat fraction using the method accounting for short T_2* species was determined as the ratio of all the fat peaks (A, B, D, E and F) area with the sum of all the fat peaks and the narrow (long T_2*) water peak area (i.e. excluding the broad-short T_2* water peak area).

To investigate chemical shift displacement effects, MRS fitting was performed using the method accounting for short T_2* species: (i) for the spectra acquired with center frequency at main fat peak, (ii) for the spectra acquired with center frequency at water peak, and (iii) for the combined spectra, formed to minimize chemical shift displacement effects. Fat fraction values were computed for all the three different options of the acquisition center frequency.

Imaging-based fat quantification

The gradient echo imaging data were reconstructed on the scanner using an online version of the algorithm labeled as iterative decomposition of water and fat with echo asymmetry and least-squares estimation (IDEAL) to perform water-fat separation (24,25). The IDEAL algorithm combined with a fat signal model accounting for the multiple peaks of the fat spectrum (as determined by the relative peak areas computed in the present fat spectrum characterization step) and a single T_2* correction was first used to derive proton density fat fraction maps (15). The derived fat fraction maps were used for guiding the positioning of the MRS voxels on the scanner in order to derive MR spectra at different red and yellow marrow locations with fat fraction values within the entire range of the observed fat fraction values.

The gradient echo imaging data were also processed off-line using in house-built routines written in MATLAB (Mathworks, Natick, MA). Specifically, a complex-based water-fat decomposition was performed using the presently determined pre-calibrated fat spectrum and single T_2* correction for the mean complex SPGR signal over the region of interest determined by the borders of the voxel of the MRS acquisition. The imaging-based fat fraction value was computed as the ratio of the mean fat signal with the sum of mean fat and water signals. There was no magnitude-induced noise bias or eddy current correction performed on the imaging-based fat quantification performed off-line.

Methods agreement analysis

The fat fraction values obtained with the two MRS-based methods (not accounting and accounting for short T_2* water species) were plotted against the fat fraction values obtained using water-fat imaging. A linear regression analysis was performed to determine the correlation (R^2), slope, and intercept as measures of agreement between fat and water fraction values obtained using water-fat imaging and the two MRS-based methods. Two-sided t tests at a significance level of p=0.05 were used to determine whether the estimated slope and intercept were statistically different from 1.0 and 0.0, respectively.

RESULTS

Figure 1 shows the peak area results used in the characterization of the fat spectrum. By performing a linear regression between the area of peak C and the area of peaks A+B (Fig. 1b), the intercept was found not statistically significantly different from zero (p=0.13) and the ratio of area of peak C to area of peaks A+B was determined equal to 0.201. By performing a linear regression between the area of peak D and the area of peak C (Fig. 1c), the intercept was found not statistically significantly different from zero (p=0.71) and the ratio of area of peak D to area of peak C was determined equal to 0.178. Based on these values, assuming a triglyceride chain length CL equal to 18.4 and using the model for the triglycerides structure adopted by Hamilton (22), it can then be computed that ndb = 3.8 and nmidb = 1.4. Based on the derived triglyceride chemical structure, the area of peak E and the area of peak F were determined equal to 5.4% and 10.2% respectively of the area of peaks A +B. Therefore, the computed mean fat spectrum was composed of peaks at frequency locations 0.9 ppm, 1.30 ppm, 1.59 ppm, 2.00 ppm, 2.25 ppm, 2.77 ppm, 4.2 ppm and 5.31 ppm with relative peak areas 8.7%, 56.8 %, 5.8%, 9.2%, 5.8%, 2.7%, 3.8% and 7.3% respectively.

The T_2 values for the water and fat peaks based on the MRS data processing accounting for the short T_2* species were 19.1±2.6 ms and 64.7±2.3 ms respectively (mean and standard deviation values determined over the 25 acquired MR spectra). The linewidths of the water and main fat peak were 0.44±0.04 ppm and 0.39±0.06 ppm respectively (mean and standard deviation values determined over the spectra with fat fraction below 85%). The difference between the water and main fat peak linewidth was 0.06±0.06 ppm and thus statistically significantly different from 0 (p=0.004).

Fig. 1a shows an example of the chemical shift displacement effect on the bone marrow MR spectrum in the proximal femur. Both the main fat peak B and the water peak areas were affected by the center frequency of the acquired MR spectrum. Fig. 2a shows the T_2-corrected fat fraction results for MR spectra acquired with center frequency at main fat peak and at water peak as a function of the fat fraction results for the combined MR spectra. Considering the fat fraction results for the combined MR spectra as minimally affected by chemical shift displacement effects, chemical shift displacement effects induced a bias up to 6% on the fat fraction determined using the presently employed single-voxel MRS acquisition.

Figure 3 highlights the effect of short T_2* water species on MRS peak fitting. The fitting of the MRS data using the model not accounting for short T_2* water species shows poor agreement with the experimental MR spectra in the frequency region between 3 ppm and 4 ppm (arrows in Fig. 3a and 3d). The fitting of the MRS data using the model accounting for short T_2* water species shows good agreement with the experimental MR spectra even in the frequency region between 3 ppm and 4 ppm (arrows in Fig. 3b and 3e).

Figure 4b compares the magnitude of the measured gradient echo signal with the magnitude of the T_2-corrected MRS time-domain signal accounting for short T_2* species, and the magnitude of the T_2-corrected MRS time-domain signal not accounting for short T_2*

species. The presently employed six-echo SPGR sequence samples the signal at TE longer than 2.1 ms, where most of the gradient echo signal of the short T_2* species has already significantly decayed. For TE longer than 2.1 ms, there is therefore very good agreement between the time evolution of the T_2-corrected MRS signal with either accounting or not accounting for short T_2* species (Fig. 4b). However, for TE shorter than 2.1 ms there is a difference between the T_2-corrected MRS signal accounting for short T_2* species and the T_2-corrected MRS signal not accounting for short T_2* species (Fig. 4b).

Figure 5 compares the imaging-based fat fraction results with the MRS-based fat fraction results using the methodologies accounting and not accounting for short T_2* species. The best equivalency between MR imaging and MR spectroscopy fat fraction was reported when accounting for the effect of short T_2* species in MRS. Specifically, the results showed that there was a significant overestimation of the water fraction using the MRS model not accounting for short T_2* species with respect to the imaging-based water fraction (R^2=0.92), with a slope of 1.03±0.06 (p=0.64) and an intercept of 5.2%±1.3% (p<0.001). However, a good agreement was observed between the water fraction using the MRS model accounting for short T_2* species and the imaging-based water fraction (R^2=0.87), with a slope of 1.04±0.08 (p=0.68) and an intercept of -1.0%±1.8% (p=0.58).

DISCUSSION

The presence of trabecular bone complicates fat quantification in bone marrow using either chemical shift-based water-fat separation or single-voxel MRS. Trabecular bone shortens the T_2* relaxation time of all compartments in bone marrow, resulting in broad peaks in single-voxel MRS and a rapid gradient echo signal decay with echo time in chemical shift-based water-fat separation. In addition, short T_2* but long T_2 water components contribute to broad baseline peaks in the bone marrow MR spectrum, whereas their signal is very small at the echo times of clinically accessible gradient echo imaging. The present work proposes a methodology addressing the effect of broad peaks in MRS-based bone marrow fat quantification and the effect of short T_2* water components with the objective to perform a comparison of bone marrow fat quantification between water-fat imaging and single-voxel MRS. Based on the described methodology and after accounting for the effect of short T_2* water species in MRS a good agreement was presently found between the imaging and MRS determined fat fractions.

The hematopoietic red bone marrow distribution is spatially varying in the proximal femur. Chemical shift displacement effects in single-voxel MRS localization can induce an overestimation or underestimation of fat fraction depending on the fat content distribution in the region surrounding the MRS voxel. A displacement equal to 18% of the voxel size should be expected in one dimension for the presently employed RF pulse bandwidth of 2.4 kHz at 3 T. Chemical shift displacement effects induced a bias up to 6% in the fat fraction estimation of the proximal femur in the present data. An acquisition with two center frequencies is expected to minimize water-fat chemical shift displacements, especially when applying single-voxel MRS in regions with spatially inhomogeneous fat content or close to the border between bone marrow and other tissues.

The broad overlapping water and fat peaks in the region from 3 ppm to 6 ppm complicate the accurate extraction of water and total fat components. The characterization of the chemical structure of the bone marrow triglycerides (22) makes the water peak extraction less sensitive to the occurrence of overlapping water and fat peaks in the presence of thin trabecular bone structures. Based on the analysis of the 25 presently acquired spectra, the mean bone marrow fat spectrum was found to have higher ndb and nmidb values and thus higher relative area for the olefinic peak F compared to the previously reported liver fat spectrum (22).

A rigorous comparison of the bone marrow fat fraction measurement between single-voxel MRS and water-fat imaging should consider the effect of short T_2* species. The single-voxel STEAM-MRS acquisition window starts sampling the free-induction decay (FID) signal at very short time intervals after the formation of the stimulated echo. Therefore, the MRS FID signal in general includes signal contributions from short T_2* species. Clinically accessible gradient echo imaging measures the signal at TEs longer than 1-2 ms. Therefore, the gradient echo signal does not in general include significant signal contributions from short T_2* species (26,27). When the MRS model does not account for the presence of the short T_2* species, the area of the short T_2* species ends up being considered within the water peak area inducing an underestimation of the MRS-based fat fraction compared to the imaging-based fat fraction. Therefore, the present preliminary data suggest that in order to compare the fat fraction measurements between water-fat imaging and single-voxel MRS, the MRS data processing should use a model accounting for short T_2* species and exclude the determined area of the short T_2* species in the calculation of the fat fraction. After accounting for the effect of short T_2* species a good equivalency was presently found between imaging-based and MRS-based fat fractions. However, the correlation coefficient between the imaging-based fat fraction and the MRS-based fat fraction accounting for short T_2* species was lower than the correlation coefficient between the imaging-based fat fraction and the MRS-based fat fraction not accounting for short T_2* species. That could be attributed to the need for fitting additional unknowns while extracting the broad water peak in the MRS data processing accounting for short T_2* species.

The present study has some limitations. First, a constant fat spectrum was assumed for all bone marrow locations in all subjects. Although some variation might be expected in the unsaturation index across subjects (28), the assumption of a constant fat spectrum model invariant across subjects should be a good first approximation while focusing on fat fraction quantification. Second, the imaging-based fat fraction was determined by first averaging the complex signal over the studied region of interest and then performing the chemical shift-based water-fat separation on the averaged complex signal. Such an approach was preferred instead of the approach preforming first chemical shift-based water-fat separation on a voxel-by-voxel basis and then averaging the fat fraction over the region of interest to avoid magnitude-induced noise bias effects on the fat fraction (18). Specifically, given the large T_1 value difference between water and fat in bone marrow (29), a low flip angle was selected to reduce T_1-bias effects (14,17,18), reducing the overall imaging SNR (17,18). A voxel-by-voxel chemical shift-based water-fat separation in femur regions with short T_2* and thus low local SNR at the late TEs of the gradient-echo acquisition would then suffer from a noise-induced underestimation of the fat fraction at high fat fractions (18). By averaging first the

signal over the region of interest magnitude-induced noise bias effects could be minimized. Third, the present results simply report on the presence of a broad water peak in the MR spectrum without providing any evidence on the source of this broad water peak. Such short T_2* water components could be arising from water molecules within trabecular bone pores with different scales or water molecules affected by the presence of macromolecules or paramagnetic ions. A rigorous analysis of imaging and MRS data acquired in red bone marrow specimens at clinically-accessible and ultra-short echo times would be required to understand the source of the observed short T_2* water components, as previously performed in cortical bone (30). Fourth, a single T_2* correction was adopted in the solution of the water-fat separation problem based on the imaging data. The MRS-derived results show that the linewidth of the water is statistically significantly higher than the linewidth of the main fat peak, suggesting a difference in the relative T_2* values between the water and the main fat peak. However, further work would be required in order to compare the accuracy and noise performance of single versus dual T_2* correction methods in quantitative water-fat imaging of bone marrow, as previously performed in the liver (31,32). Finally, the number of the subjects studied in the present study is relatively small and parts of the MRS measurements are not fully independent, as they belong to the same subject. The characterization of the bone marrow fat spectrum, the assessment of the accuracy of singe and dual T_2* correction on bone marrow water-fat separation, and the comparison of fat fraction accuracy and precision between water-fat imaging and single-voxel MRS would benefit from a larger scale study.

Fat content measurements using chemical shift-based water-fat separation have shown good agreement with fat content measurements using single-voxel MRS in different body parts (10-12). The present work emphasizes on the need to account for short T_2* water species when comparing fat content measurements using water-fat imaging and single-voxel MRS in bone marrow in the presence of trabecular bone. Specifically, the MR visible signal in clinically accessible gradient echo imaging does not include the contribution of signal from water species with short T_2*. The signal of such species would contribute to the signal of imaging sequences only in sequences with ultra-short echo time capabilities.

CONCLUSIONS

Bone marrow fat quantification in the presence of trabecular bone using single-voxel MRS should use a methodology accounting for short T_2* water species and exclude the determined area of the short T_2* water species in the calculation of the fat fraction while comparing it with imaging-based fat fraction. After accounting for the effect of short T_2* water species a good equivalency was presently found between imaging-based and MRS-based fat fractions in the proximal femur of healthy volunteers.

Acknowledgments

The authors would like to thank Ann Shimakawa (GE Healthcare) for her valuable help with the water-fat imaging pulse sequence. The present research was supported by NIH-R01 AR057336.

References

1. Baum T, Yap SP, Karampinos DC, Nardo L, Kuo D, Burghardt AJ, Masharani UB, Schwartz AV, Li X, Link TM. Does vertebral bone marrow fat content correlate with abdominal adipose tissue, lumbar spine bone mineral density, and blood biomarkers in women with type 2 diabetes mellitus? J Magn Reson Imaging. 2012; 35(1):117–124. [PubMed: 22190287]
2. Griffith JF, Yeung DKW, Antonio GE, Lee FKH, Hong AWL, Wong SYS, Lau EMC, Leung PC. Vertebral bone mineral density, marrow perfusion, and fat content in healthy men and men with osteoporosis: dynamic contrast-enhanced MR imaging and MR spectroscopy. Radiology. 2005; 236(3):945–951. [PubMed: 16055699]
3. Griffith JF, Yeung DKW, Antonio GE, Wong SYS, Kwok TCY, Woo J, Leung PC. Vertebral marrow fat content and diffusion and perfusion indexes in women with varying bone density: MR evaluation. Radiology. 2006; 241(3):831–838. [PubMed: 17053202]
4. Pichardo JC, Milner RJ, Bolch WE. MRI measurement of bone marrow cellularity for radiation dosimetry. J Nucl Med. 2011; 52(9):1482–1489. [PubMed: 21799087]
5. Li X, Kuo D, Schafer AL, Porzig A, Link TM, Black D, Schwartz AV. Quantification of vertebral bone marrow fat content using 3 Tesla MR spectroscopy: reproducibility, vertebral variation, and applications in osteoporosis. J Magn Reson Imaging. 2011; 33(4):974–979. [PubMed: 21448966]
6. Schick F, Bongers H, Jung WI, Skalej M, Lutz O, Claussen CD. Volume-selective proton MRS in vertebral bodies. Magn Reson Med. 1992; 26(2):207–217. [PubMed: 1513248]
7. Reeder SB, Cruite I, Hamilton G, Sirlin CB. Quantitative assessment of liver fat with magnetic resonance imaging and spectroscopy. J Magn Reson Imaging. 2011; 34(4):729–749. [PubMed: 21928307]
8. Reeder SB, Hu HH, Sirlin CB. Proton density fat-fraction: A standardized MR-based biomarker of tissue fat concentration. J Magn Reson Imaging. 2012; 36:1011–1014. [PubMed: 22777847]
9. Hines CD, Frydrychowicz A, Hamilton G, Tudorascu DL, Vigen KK, Yu H, McKenzie CA, Sirlin CB, Brittain JH, Reeder SB. T(1) independent, T(2) (*) corrected chemical shift based fat-water separation with multi-peak fat spectral modeling is an accurate and precise measure of hepatic steatosis. J Magn Reson Imaging. 2011; 33(4):873–881. [PubMed: 21448952]
10. Hu HH, Kim HW, Nayak KS, Goran MI. Comparison of fat-water MRI and single-voxel MRS in the assessment of hepatic and pancreatic fat fractions in humans. Obesity (Silver Spring). 2010; 18:841–847. [PubMed: 19834463]
11. Meisamy S, Hines CD, Hamilton G, Sirlin CB, McKenzie CA, Yu H, Brittain JH, Reeder SB. Quantification of hepatic steatosis with T1-independent, T2*-corrected MR imaging with spectral modeling of fat: blinded comparison with MR spectroscopy. Radiology. 2011; 258:767–775. [PubMed: 21248233]
12. Yokoo T, Shiehmorteza M, Hamilton G, Wolfson T, Schroeder ME, Middleton MS, Bydder M, Gamst AC, Kono Y, Kuo A, Patton HM, Horgan S, Lavine JE, Schwimmer JB, Sirlin CB. Estimation of hepatic proton-density fat fraction by using MR imaging at 3.0 T. Radiology. 2011; 258(3):749–759. [PubMed: 21212366]
13. Hernando D, Haldar JP, Sutton BP, Ma J, Kellman P, Liang ZP. Joint estimation of water/fat images and field inhomogeneity map. Magn Reson Med. 2008; 59(3):571–580. [PubMed: 18306409]
14. Bydder M, Yokoo T, Hamilton G, Middleton MS, Chavez AD, Schwimmer JB, Lavine JE, Sirlin CB. Relaxation effects in the quantification of fat using gradient echo imaging. Magn Reson Imaging. 2008; 26(3):347–359. [PubMed: 18093781]
15. Yu H, Shimakawa A, McKenzie CA, Brodsky E, Brittain JH, Reeder SB. Multiecho water-fat separation and simultaneous R_2* estimation with multifrequency fat spectrum modeling. Magn Reson Med. 2008; 60(5):1122–1134. [PubMed: 18956464]
16. Yu H, McKenzie CA, Shimakawa A, Vu AT, Brau AC, Beatty PJ, Pineda AR, Brittain JH, Reeder SB. Multiecho reconstruction for simultaneous water-fat decomposition and T_2* estimation. J Magn Reson Imaging. 2007; 26(4):1153–1161. [PubMed: 17896369]

17. Karampinos DC, Yu H, Shimakawa A, Link TM, Majumdar S. T1-corrected fat quantification using chemical shift-based water/fat separation: application to skeletal muscle. Magn Reson Med. 2011; 66:1312–1326. [PubMed: 21452279]
18. Liu CY, McKenzie CA, Yu H, Brittain JH, Reeder SB. Fat quantification with IDEAL gradient echo imaging: correction of bias from T_1 and noise. Magn Reson Med. 2007; 58(2):354–364. [PubMed: 17654578]
19. Hernando D, Hines CD, Yu H, Reeder SB. Addressing phase errors in fat-water imaging using a mixed magnitude/complex fitting method. Magn Reson Med. 2012; 67:638–644. [PubMed: 21713978]
20. Yu H, Shimakawa A, Hines CDG, McKenzie CA, Hamilton G, Sirlin CB, Brittain JH, Reeder SB. Combination of complex-based and magnitude-based multiecho water-fat separation for accurate quantification on fat-fraction. Magn Reson Med. 2011; 66:199–206. [PubMed: 21695724]
21. Karampinos DC, Yu H, Shimakawa A, Link TM, Majumdar S. Chemical shift-based water/fat separation in the presence of susceptibility-induced fat resonance shift. Magn Reson Med. 2012; 68(5):1495–1505. [PubMed: 22247024]
22. Hamilton G, Yokoo T, Bydder M, Cruite I, Schroeder ME, Sirlin CB, Middleton MS. In vivo characterization of the liver fat ^{1}H MR spectrum. NMR Biomed. 2011; 24(7):784–790. [PubMed: 21834002]
23. Reeder SB, Robson PM, Yu H, Shimakawa A, Hines CDG, McKenzie CA, Brittain JH. Quantification of hepatic steatosis with MRI: the effects of accurate fat spectral modeling. J Magn Reson Imaging. 2009; 29(6):1332–1339. [PubMed: 19472390]
24. Reeder SB, Pineda AR, Wen Z, Shimakawa A, Yu H, Brittain JH, Gold GE, Beaulieu CH, Pelc NJ. Iterative decomposition of water and fat with echo asymmetry and least-squares estimation (IDEAL): application with fast spin-echo imaging. Magn Reson Med. 2005; 54(3):636–644. [PubMed: 16092103]
25. Reeder SB, Wen Z, Yu H, Pineda AR, Gold GE, Markl M, Pelc NJ. Multicoil Dixon chemical species separation with an iterative least-squares estimation method. Magn Reson Med. 2004; 51(1):35–45. [PubMed: 14705043]
26. Hu HH, Li Y, Nagy TR, Goran MI, Nayak KS. Quantification of absolute fat mass by magnetic resonance imaging: a validation study against chemical analysis. Int J Body Compos Res. 2011; 9(3):111–122. [PubMed: 23204926]
27. Reeder, SB.; Hines, CD.; Yu, H.; McKenzie, CA.; Brittain, JH. Relationship between proton-density fat-fraction and true fat concentration for in vivo fat quantification with magnetic resonance imaging. Proceedings of the 19th Annual Meeting of ISMRM Montreal; Canada. 2011. p. 805
28. Yeung DKW, Griffith JF, Antonio GE, Lee FKH, Woo J, Leung PC. Osteoporosis is associated with increased marrow fat content and decreased marrow fat unsaturation: a proton MR spectroscopy study. J Magn Reson Imaging. 2005; 22(2):279–285. [PubMed: 16028245]
29. Schick F, Bongers H, Jung W-I, Eismann B, Skalej M, Einsele H, Lutz O, Claussen CD. Proton relaxation times in human red bone marrow by volume selective magnetic resonance spectroscopy. Appl Magn Reson. 1992; 3:947–963.
30. Horch RA, Nyman JS, Gochberg DF, Dortch RD, Does MD. Characterization of 1H NMR signal in human cortical bone for magnetic resonance imaging. Magn Reson Med. 2010; 64(3):680–687. [PubMed: 20806375]
31. Horng DE, Hernando D, Hines CD, Reeder SB. Comparison of R2* correction methods for accurate fat quantification in fatty liver. J Magn Reson Imaging. 2013; 37(2):414–422. [PubMed: 23165934]
32. Reeder SB, Bice EK, Yu H, Hernando D, Pineda AR. On the performance of T(2) * correction methods for quantification of hepatic fat content. Magn Reson Med. 2012; 67(2):389–404. [PubMed: 21661045]

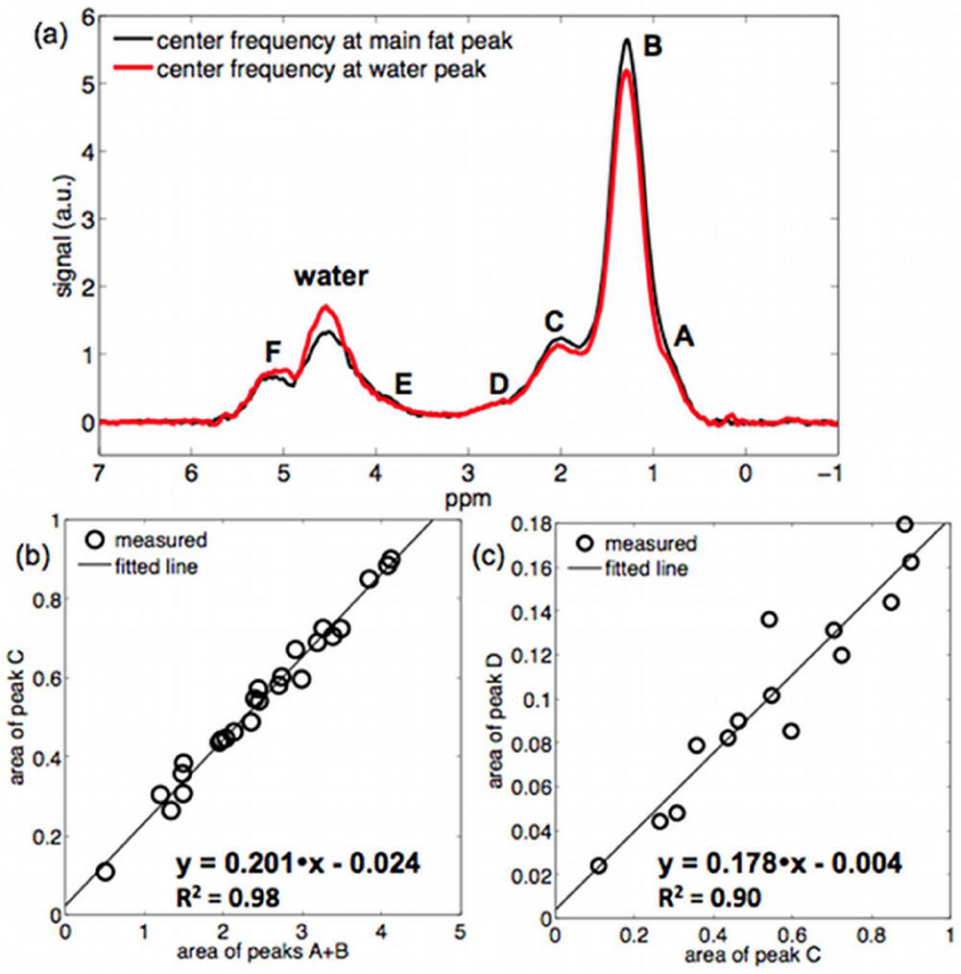

Figure 1.

Model of bone marrow triglyceride structure: (a) typical proximal femur MR spectrum (acquisitions with center frequency at the main fat peak and at the water peak), (b) relationship between area of peak C and area of peaks A+B (for all acquired spectra with center frequency at the main fat peak), and (c) relationship between area of peak D and area of peak C (for spectra with center frequency at the main fat peak and with fat peak linewidth smaller than 0.4 ppm).

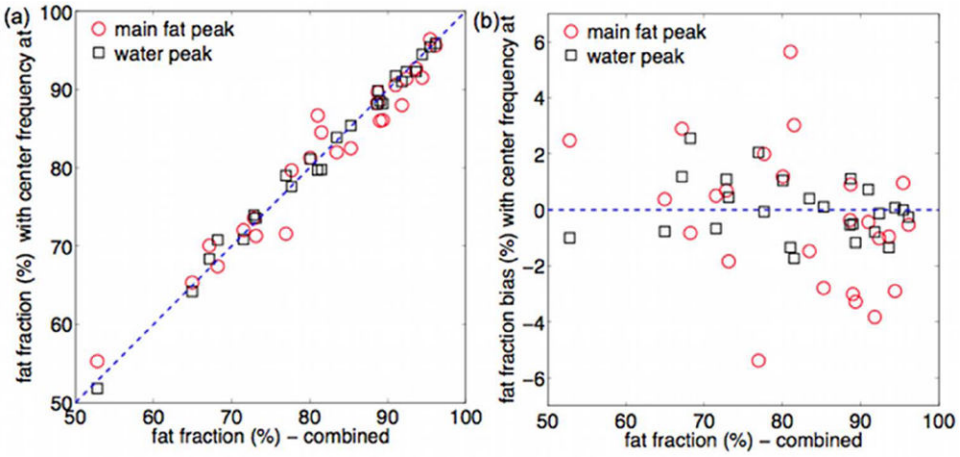

Figure 2.

Chemical shift displacement effect on MRS-based fat fraction: (a) relationship between fat fraction based on combined spectra and fat fraction based on acquisitions with center frequency on the main fat peak and on the water peak (the dashed line represents the unity), and (b) corresponding fat fraction bias (the dashed line represents zero bias).

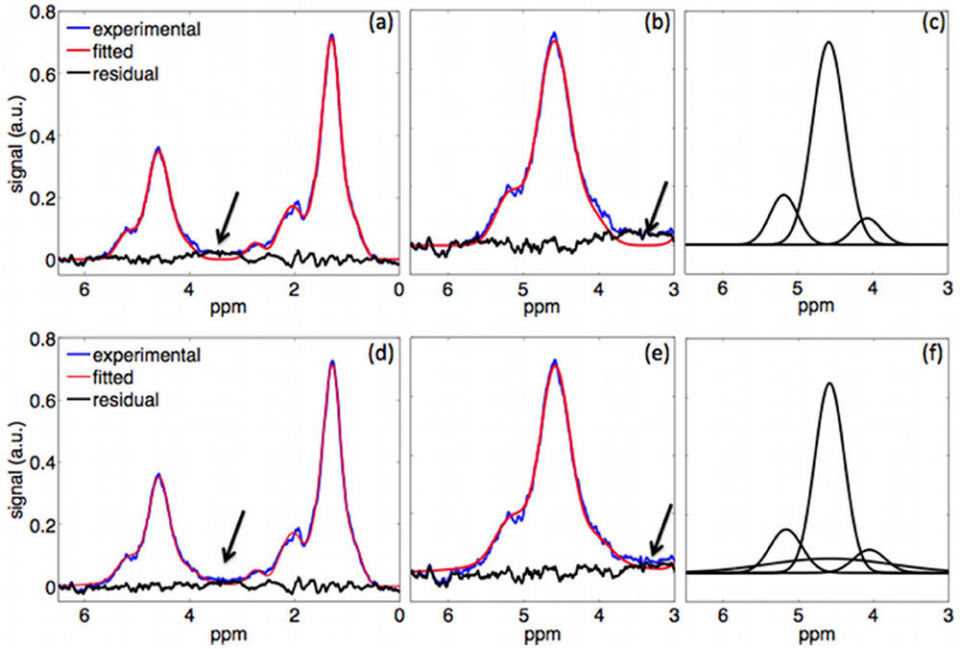

Figure 3.

Bone marrow MR spectra using fitting not accounting for short T_2* water species (a-c) and accounting for short T_2* water species (d-f): (a) and (d) full spectra, (b) and (e) spectra zoomed in water peak region, (c) and (f) superposition of decomposed modeled peaks in water peak region.

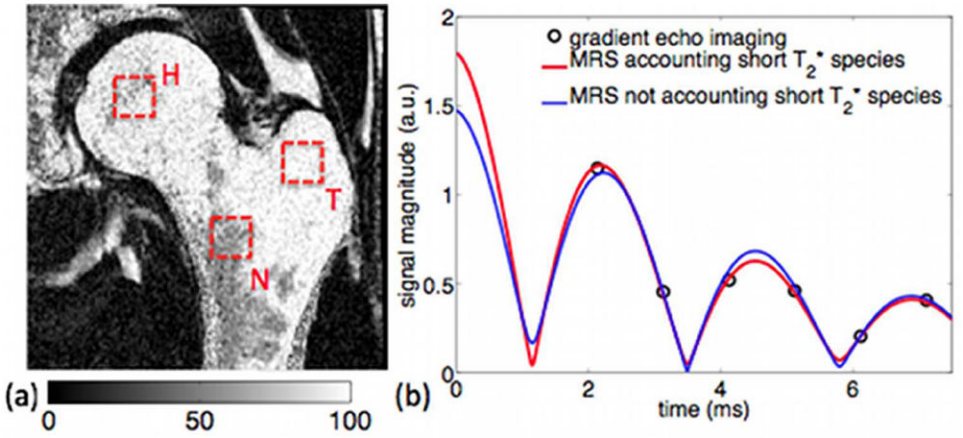

Figure 4.

(a) Imaging-based fat fraction map and typical MRS voxel locations in neck (N), greater trochanter (T) and head regions (H), and (b) time evolution of magnitude signal: experimental gradient echo imaging signal, fitted T_2-corrected MRS time domain signal accounting for short T_2* water species, and fitted T_2-corrected MRS time domain signal not accounting for short T_2* water species.

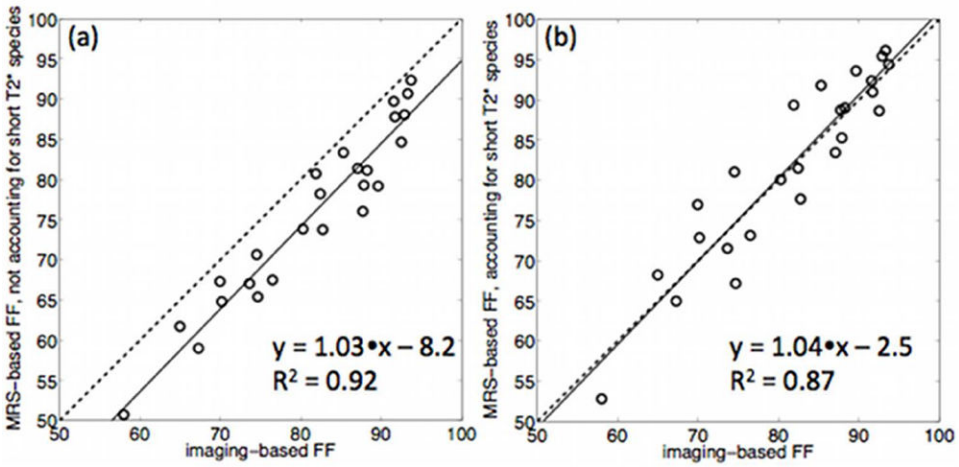

Figure 5.

Fat fraction (FF) results comparison between: (a) water-fat imaging and MRS with fitting not accounting for short T_2* species, and (b) water-fat imaging and MRS with fitting accounting for short T_2* species. The solid line represents the linear fit derived from linear regression analysis and the dashed line represents the unity.